Coherent transients excited by subpicosecond pulses of terahertz radiation

H. Harde* and D. Grischkowsky

IBM Watson Research Center, P.O. Box 218, Yorktown Heights, New York 10598

Using a newly developed optoelectronic source of well-collimated beams of subpicosecond pulses of terahertz radiation to excite a N_2O vapor cell, we have observed the subsequent emission from the vapor of a coherent pulse train extending as long as 1 ns. The individual subpicosecond terahertz pulses of the train are separated by 39.8 ps, corresponding to the frequency separation between adjacent rotational lines of the excited manifold of more than 50 lines. From these observations the coherent relaxation time T_2 is obtained as a function of vapor pressure, even for the case of overlapping lines. In addition, from the pulse repetition rate in the train the frequency separation between the rotational lines is determined. Finally, from the changing individual pulse shapes in the train the anharmonicity factor for the N_2O molecule is evaluated.

1. INTRODUCTION

Coherent transient effects resulting from the interaction of electromagnetic radiation with resonant systems were first studied for nuclear- and paramagnetic-spin systems at radio and microwave frequencies.[1] Analogous studies in the optical regime were initiated with the photon echo experiment,[2] and since that time there have been extensive studies of coherent effects in both the visible and infrared regimes.[3-5] While many of these phenomena are the analogs of effects first observed in spin resonance, some of them do not have a spin-resonance counterpart, because of propagation effects and the fact that in the optical regime the samples are usually large compared with a wavelength. For these effects the full coupled Maxwell–Bloch system is involved. Coherent transients allow for the study of the dynamics involved in the interaction of radiation and matter but also can be used successfully for high-precision measurements of frequency splittings between atomic substates[6,7] or for the investigations of relaxation processes.[5,8]

In this paper we report an experimental and theoretical study of coherent effects in the terahertz frequency range by exciting N_2O molecules and detecting the free-induction decay (FID) reradiated by the vapor. This newly accessible frequency range, midway between the frequencies used for spin resonance and those of infrared and optical studies, is important owing both to the samples that can be investigated and to the unusual experimental conditions encountered with subpicosecond pulses of terahertz radiation. The recently developed optoelectronic terahertz beam system used in the experiment produces subpicosecond pulses of terahertz radiation that are well collimated into low-divergence beams.[9-13] These pulses of terahertz electromagnetic radiation can be detected with signal-to-noise (S/N) ratios of better than 10,000. Compared with previous studies of coherence effects in the radio frequency and microwave regimes for nuclear- and electron-spin systems (see, e.g., Ref. 1), the research reported here involves samples that are many wavelengths in length, so that, in addition to the point response, propa-

gation effects are also important. In contrast with investigations at infrared and optical frequencies, where coherent transients are detected only as pulse intensities or as beat notes on a carrier,[4,5,14] our experiments directly measure the actual electric field of the transmitted radiation pulse and that radiated by the coherent response of the sample. This feature allows for experimental studies with unprecedented precision, and both the amplitude and the phase are measured within the broad bandwidth of the terahertz pulse extending from low frequencies up to 2 THz. Because the frequency changes by more than ten times from the lowest to the highest values, it is not appropriate to describe these pulses by a carrier frequency and a time-dependent envelope, as is usually done in the infrared and visible regions. This situation precludes the use of the concept of pulse area for pulse propagation effects, and also the slowly varying envelope approximation of coherent optics cannot be applied for pulses that essentially consist of only a single cycle. Thus some measurements of coherent terahertz propagation effects require an extended theory for their understanding; for example, it is not clear whether self-induced transparency can even occur under these conditions.

The propagation of these terahertz pulses through N_2O vapor excites a multitude of rotational transitions in the impact approximation and causes the molecules to reradiate a FID signal that consists of a series of uniformly spaced subpicosecond terahertz pulses (for a similar phenomenon of emitted infrared pulses after excitation see Refs. 15 and 16). We have measured, with a time resolution of better than 0.5 ps, trains of pulses extending to beyond 600 ps. These measurements are compared with theoretical simulations that we derived by solving the wave equation for the propagation of the terahertz pulses through the vapor. These calculations were based on linear dispersion theory, where the linear response of the molecules to the propagating terahertz pulses was obtained in the frequency domain, and from the resulting spectral response the time-domain behavior was determined. A fit of the calculated pulse structure to the measurements directly determined the homogeneous re-
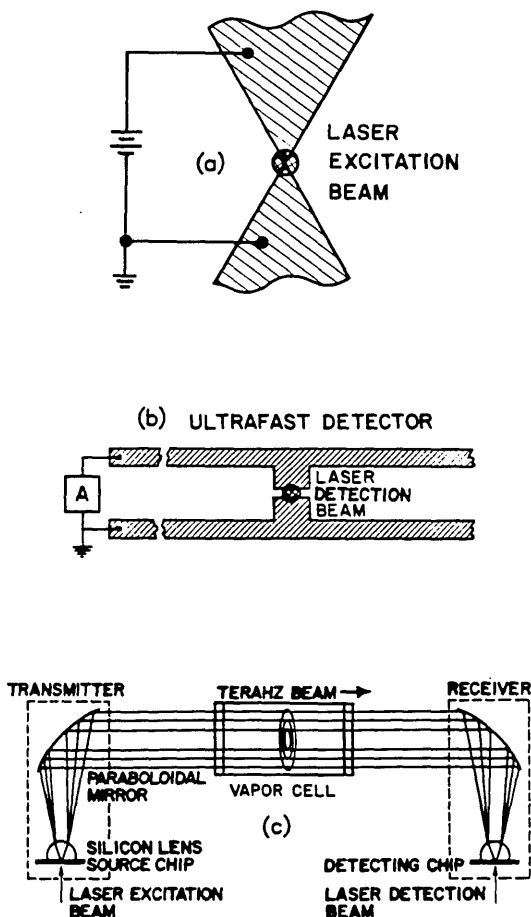
Fig. 1. Experimental setup of the terahertz radiation source and detection system with (a) bow-tie transmitting antenna, (b) ultrafast receiving antenna, and (c) terahertz optics.

laxation time T_2 as a function of vapor pressure up to values for which in the frequency domain the absorption lines would be completely overlapping. From the pulse repetition rate in the train the frequency separation between the rotational lines was determined, and, because of the exceptionally high time resolution of the measurements, an anharmonicity in the line spacing was detected as reshaping of the individual pulses in the train.

2. EXPERIMENTAL SETUP

The terahertz radiation source is illustrated in Fig. 1(a). Here the emitting antenna has a 60° bow-tie geometry with a 5 μm × 5 μm photoconductive gap. The bow tie extends 2 mm in both directions to parallel electrode lines separated by 4 mm. Compared with our previous transmitting antennas,[9-13] the bow-tie geometry generates a stronger signal that is richer in low-frequency components. The antenna was fabricated on an intrinsic, high-resistivity (greater than 10 MΩ-cm) gallium arsenide wafer. The antenna, biased at 10 V, was driven by photoconductive shorting of the antenna gap with 70-fs pulses coming at a 100-MHz rate in a 6-mW beam from a colliding-pulse, mode-locked dye laser. The terahertz radiation detector uses the ultrafast antenna and terminating transmission line geometry illustrated in Fig. 1(b). This receiving antenna was located in the middle of a 20-mm-long transmission line consisting of two parallel

10-μm-wide aluminum lines separated by 30 μm. This detector was fabricated on an ion-implanted, silicon-on-sapphire wafer. During operation the receiving antenna is driven by the incoming terahertz radiation pulse polarized parallel to the antenna. We measured the induced time-dependent voltage across the 5-μm-wide antenna gap by shorting the gap with the 70-fs optical pulses in the 5-mW detection beam and monitoring the collected charge (current) versus the time delay between the excitation and detection laser pulses.

The terahertz optics illustrated in Fig. 1(c) consist of two matched crystalline silicon spherical lenses contacted to the back side of the gallium arsenide emitting and silicon-on-sapphire detecting chips located near the foci of two identical paraboloidal mirrors. The combination of the silicon lens and the paraboloidal mirror collimated the emitted radiation to beam diameters proportional to the wavelength and with a frequency-independent divergence of 25 mrad. The second identical combination on the receiving end focused the terahertz beam on the detector. The total path length from transmitter to receiver was 88 cm, of which 86 cm was located in an airtight enclosure. During our measurements the enclosure was filled with dry nitrogen to mitigate the effects of water vapor on the terahertz beams.

The measured transmitted terahertz pulse is displayed in Fig. 2(a), where the maximum-to-minimum time separation is seen to be 0.85 ps. This is significantly broader than that obtained for the earlier systems,[9-13] which used the antenna geometry of Fig. 1(b) for the transmitter, instead of the bow-tie geometry used here. The corresponding amplitude spectrum, obtained by a numerical Fourier transform of Fig. 2(a), is displayed in Fig. 2(b). The spec-
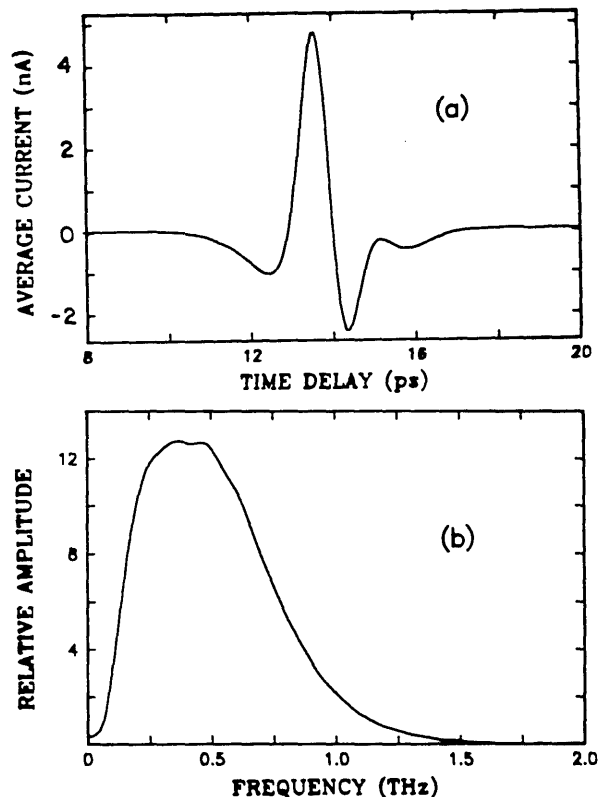

Fig. 2. (a) Measured transmitted terahertz pulse and (b) amplitude spectrum of the measured pulse of (a).
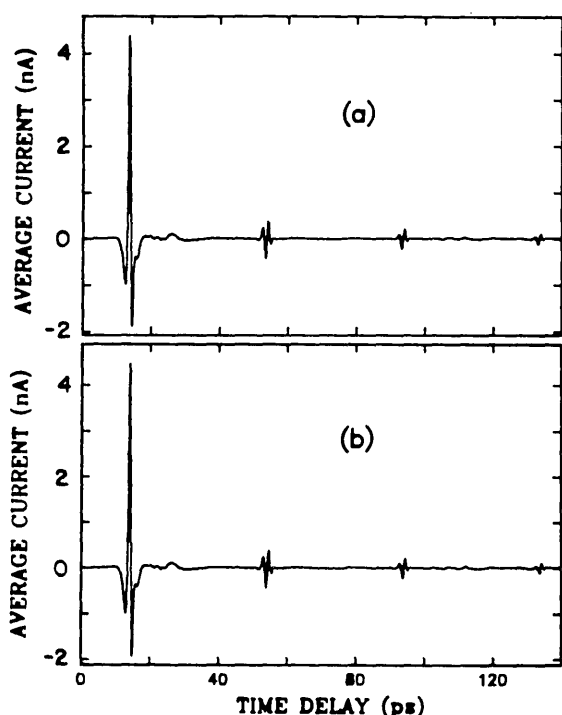
Fig. 3. (a) Measured transmitted terahertz pulse for 800 hPa of N_2O vapor and (b) corresponding calculated transmitted terahertz pulse.

trum is exceptionally smooth and extends to lower frequencies than that of the previous studies.

The measurements were performed with the N_2O vapor cell inside the airtight enclosure. The cell was constructed of stainless steel, and, in order to reduce the complicating effects of multiple reflections from the cell windows, we used 2-cm-thick, 5-cm-diameter, high-resistivity (10-kΩ-cm) silicon windows. Silicon is an ideal window material, owing to its almost complete transparency and lack of dispersion in the terahertz frequency range.[12] The length of the vapor path was 38.7 cm, and the cell had a clear aperture of 4-cm diameter.

3. N_2O MEASUREMENTS

Within the broad spectral range covered by the terahertz pulses the N_2O molecule has a multitude of pure rotational absorption lines that can be excited simultaneously in the impact approximation by the terahertz pulse. The molecules respond to this excitation by reradiating a FID signal, which decays because of relaxation, interference, and propagation effects. This is shown by the measurement presented in Fig. 3(a) for a vapor pressure of 800 hPa. Here one sees the transmitted excitation pulse followed by three coherent transients emitted by the vapor, where the relative amplitude of the first transient is 1/10 that of the excitation pulse. The theoretical comparison with this measurement is shown in Fig. 3(b). The agreement between theory and experiment is truly exceptional; every feature seen in the measurement is reproduced in the calculation. The reasons for this will be discussed in detail in Section 5. The periodicity is particularly noteworthy; during the monotonic decay, well-defined subpicosecond coherent transients appear every 40 ps. If one is to understand these observations, it is essential to realize

that the N_2O molecule is distinguished by a large number of uniformly spaced absorption lines, where to first and second orders the frequency spacing between the lines is a constant. Consequently, a periodic rephasing and dephasing of the entire ensemble of more than 50 excited transitions occurs during the FID. After the initial excitation pulse the sample emits a series of uniformly spaced subpicosecond terahertz pulses with a repetition rate of 25.1 GHz, equal to the frequency separation between adjacent lines and corresponding to a pulse separation of 39.8 ps. This situation contrasts with that of water vapor with a multitude of incommensurate resonance lines, studied earlier by terahertz time-domain spectroscopy.[10,11] The decay of the pulse train depends to first order on molecular collisions and hence on the gas pressure, while Doppler dephasing in this spectral range can be completely neglected. But, as we will discuss in Section 6, for a sample with nonnegligible optical thickness, propagation effects can cause the pulses to decay faster than the homogeneous relaxation time T_2.

When the pressure in the cell is further reduced from the value of Fig. 3, not only does the amplitude of the radiated FID become smaller but the damping of the signal is reduced as well. Owing to the experimental system's exceptionally high S/N ratio, we can then monitor the emitted pulse trains to more than 600 ps with a time resolution of better than 0.5 ps. With the cell under vacuum we obtained the output pulse shown in Fig. 4(a). Here, in addition to the main pulse, we see the reflections from the metallurgy on the transmitting antenna chip (250 ps) and the two reflections from the input and output windows (470 ps). These reflections act as additional input pulses to the N_2O vapor and subsequently generate their own coherent transient pulse trains. When the cell is filled with 120 hPa of N_2O vapor, the output pulse changes to that shown in Fig. 4(b), where the coherent pulse train emitted by the vapor is now just observable. The coherent emission is seen more clearly when we plot the difference between the measurement [Fig. 4(b)] and the reference scan [Fig. 4(a)], as Fig. 4(c) shows; the sample radiates a pulse train extending beyond the limits of the 600-ps scan of the delay time. This difference measurement procedure illustrates the importance of the high S/N ratio of the system. As we can see with 120-hPa pressure, the first coherent transient is only 1/40 the amplitude of the excitation pulse. For a S/N ratio of 10,000 with respect to the excitation pulse, the transient train can still be measured with a S/N ratio of 250. The irregular structure between the emitted transients is not noise but is due to oscillations resulting from residual water vapor. This structure did not subtract out because the water vapor pressure changed between the time the reference pulse of Fig. 4(a) was taken and the time the signal pulse of Fig. 4(b) was taken. This point is illustrated by the calculated difference structure shown in Fig. 4(d), which uses the reference pulse of Fig. 4(a) as the input. For this case the water vapor transients subtract out completely. We now demonstrate the observational power by displaying in Fig. 5 selected individual pulses of the train.

A closer look at the individual pulses of the train shows a significant reshaping of the pulses with time, as illustrated by a comparison of the 1st, 7th, and 14th coherent pulses emitted by the sample 40, 280, and 560 ps, respec-
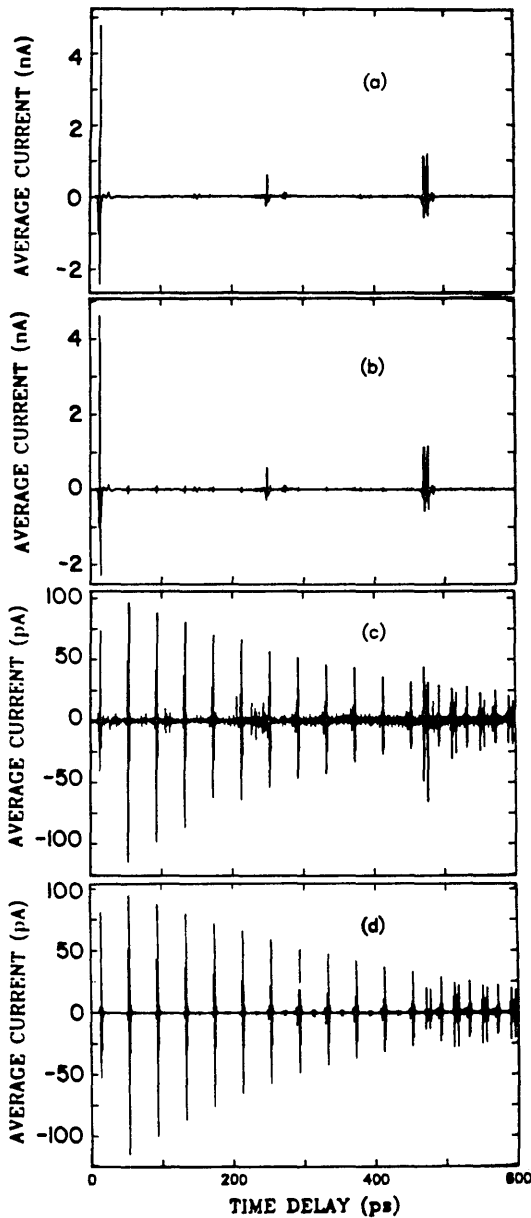
Fig. 4. (a) Reference pulse measured without N_2O in the cell, (b) measurement for 120 hPa of N_2O vapor, (c) radiated pulse train as difference of (b) and (a), and (d) calculated radiated pulse train with (a) as the input pulse.

gas and hence in the FID is washed out owing to frequency shifts resulting from the motion of the molecules, this phenomenon might be called centrifugal dephasing. To our knowledge, this is the first time that this type of dephasing has been observed in the time domain.

With the use of the theoretical approach described in Section 4 the calculated pulse shapes of the coherent transients are shown as the dashed curves in Fig. 5. The excellent agreement is obtained when we fit the pulse shape with a centrifugal stretching constant $D_V = 5.28$ kHz, as is known from the literature.[17]

4. THEORY

For a first-order theoretical description and simulation of the measurements under our experimental conditions, the sample can be represented by an entire set of uncoupled transitions, and a linear response of the sample to the exciting pulse can be assumed. In this simplified picture the input pulse excites the N_2O molecules simultaneously

tively, after the initial excitation pulse [see Figs. 5(a), 5(b), and 5(c)]. This reshaping is caused by small deviations from the rigid-rotator model of the N_2O molecules. As we discussed above, the background oscillations seen on the measurements are independent of the N_2O coherent transients. They result from the residual water vapor, which at longer delay times is additionally excited by the window reflections and therefore appear more strongly in Fig. 5(c). The system noise level, most clearly seen in Fig. 5(c), is approximately 0.5 pA. As centrifugal forces can increase the moment of inertia of a rotating molecule, the frequency spacing between adjacent rotational lines is not constant but decreases slightly with increasing rotational quantum number J. This anharmonicity causes a gradual dephasing of the individual transitions and manifests itself as a change in the coherent pulse shape. In analogy with Doppler dephasing, where the induced polarization in the
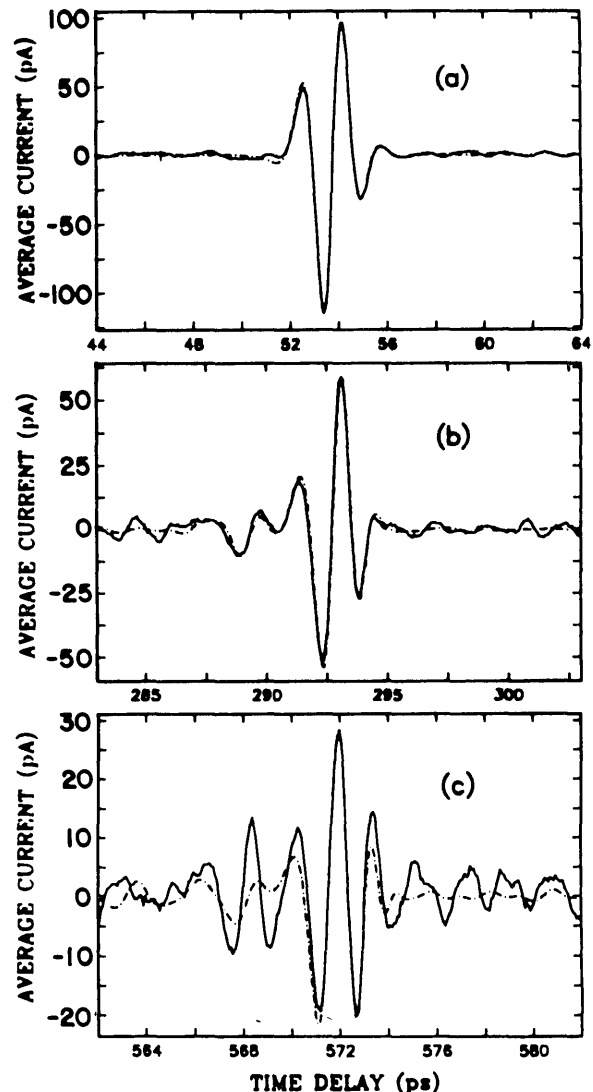

Fig. 5. Measurement (solid curve) and calculation (dashed curve) of the pulse shape of (a) the 1st, (b) the 7th, and (c) the 14th radiated coherent pulses on a magnified time scale for 120 hPa of N_2O vapor.

on the many different rotational transitions proportional to the integrated line absorption and the spectral amplitude of the initial field on a transition. Owing to this coherent excitation a phased array of dipole oscillators is formed in time and space, which radiates coherently and simultaneously with the many different frequencies of the excited rotational transitions. Therefore the radiated FID is found by a phase-sensitive summation over all the rotational transitions excited within the spectral width of the terahertz beam. This simple model makes plausible the physical origin of the observations and even permits one to simulate the radiated pulse shapes, which are in good agreement with the measurements. Only a unique phase adjustment (identical for all frequency components) is necessary to account for the shape of the exciting pulse and hence its influence on the shape of the generated pulse train. However, this simple picture is not appropriate for the description of the exciting pulse or of any propagation effects.

A more accurate description therefore requires the solution of the coupled Maxwell–Bloch equations. For a plane wave with electric field $E(z,t)$ propagating in the z direction, the wave equation can be written in SI units as

$$\frac{\partial^2 E(z,t)}{\partial z^2} - \frac{n^2}{c^2}\frac{\partial^2 E(z,t)}{\partial t^2} = \mu_0 \frac{\partial^2 P(z,t)}{\partial t^2}, \qquad (1)$$

where c is the speed of light in vacuum, μ_0 is the vacuum permeability, and $P(z,t)$ is the polarization induced in the medium by the electric field. The refractive index n in this equation represents the nonresonant interaction of the field with the sample. Because we are in the low-intensity limit of the Maxwell–Bloch equations, their solution reduces to that of linear dispersion theory.[3] We can then describe the interaction of the electric field with the sample in the frequency domain by introducing the linear polarization as

$$P(\omega) = \varepsilon_0 \chi(\omega) E(\omega), \qquad (2)$$

where ε_0 is the vacuum permittivity and $\chi(\omega) = \chi'(\omega) + i\chi''(\omega)$ is the complex electric susceptibility, the real part $\chi'(\omega)$ describing the dispersion of the medium and the imaginary part $\chi''(\omega)$ describing the absorption of the medium. The spectral distribution $E(\omega)$ is found from the Fourier transform of the initial pulse with

$$E(\omega) = \frac{1}{2\pi}\int_{-\infty}^{\infty} E(0,t)\exp(i\omega t)\mathrm{d}t. \qquad (3)$$

The electric field and the polarization in the time domain can then be represented by the inverse transformations:

$$E(z,t) = \int_{-\infty}^{\infty} E(\omega)\exp\{-i[\omega t - k(\omega)z]\}\mathrm{d}\omega \qquad (4)$$

and, with Eq. (2),

$$P(z,t) = \varepsilon_0 \int_{-\infty}^{\infty} \chi(\omega) E(\omega)\exp\{-i[\omega t - k(\omega)z]\}\mathrm{d}\omega. \qquad (5)$$

In this representation it is easily shown that the wave equation is rigorously satisfied by a propagating electromagnetic field with the wave vector

$$k(\omega) = k_0 \left[1 + \frac{\chi(\omega)}{n^2}\right]^{1/2} \simeq k_0 \left[1 + \frac{1}{2n^2}\chi'(\omega) + \frac{i}{2n^2}\chi''(\omega)\right], \qquad (6)$$

where $k_0 = \omega n/c$ is the nonresonant wave vector in the sample. As is known from linear dispersion theory, the real part of $\chi(\omega)$ changes the phase per unit length from k_0 to $k_0 + \Delta k$, with

$$\Delta k(\omega) = (k_0/2n^2)\chi'(\omega), \qquad (7)$$

and the imaginary part causes the amplitude to be exponentially attenuated with distance z according to $\exp(-\alpha z/2)$, where

$$\alpha(\omega) = (k_0/n^2)\chi''(\omega) \qquad (8)$$

is the power absorption coefficient.

So, with $\chi(\omega)$ known, the propagation of the pulse $E(z,t)$ through the sample can be calculated from Eq. (4), which with the relations of Eqs. (7) and (8) takes the form

$$E(z,t) = \int_{-\infty}^{\infty} E(\omega)\exp[-i(\omega t - k_0 z)]\exp[i\Delta k(\omega)z]$$
$$\times \exp\left[-\frac{1}{2}\alpha(\omega)z\right]\mathrm{d}\omega. \qquad (9)$$

The absorption coefficient for a single rotational transition of N_2O from J to $J + 1$, assuming unpolarized radiation and/or unoriented molecules, can be written as (for details see, e.g., Ref. 18)

$$\alpha_J(\omega) = \frac{pf_0\mu^2 h B_V \omega^2}{6nc\varepsilon_0(kT)^3}(J+1)$$
$$\times \exp\left[\frac{-hB_V J(J+1)}{kT}\right]G_A(\omega,\omega_J), \qquad (10)$$

with a Van Vleck–Weisskopf line shape

$$G_A(\omega,\omega_J) = \frac{\Delta\omega_J}{(\omega-\omega_J)^2 + (\Delta\omega_J/2)^2} + \frac{\Delta\omega_J}{(\omega+\omega_J)^2 + (\Delta\omega_J/2)^2} \qquad (11)$$

and a transition frequency

$$\omega_J/2\pi = 2B_V(J+1) - 4D_V(J+1)^3, \qquad (12)$$

where $\Delta\omega_J$ is the angular frequency linewidth (FWHM), B_V is the rotational constant of the vibrational state, D_V is the centrifugal stretching constant, p is the gas pressure, f_0 is the fraction of molecules in the lowest vibrational state, μ is the electric dipole moment, h is Planck's constant, and kT is the thermal energy.

For the change of the wave vector it is found that

$$\Delta k_J = \frac{pf_0\mu^2 h B_V \omega \omega_J^2}{3nc\varepsilon_0(kT)^3(\omega_J^2 - \omega^2)}(J+1)$$
$$\times \exp\left[\frac{-hB_V J(J+1)}{kT}\right]G_N(\omega,\omega_J), \qquad (13)$$

where

$$G_N(\omega,\omega_J) = 1 - \frac{\omega\Delta\omega_J^2}{8\omega_J^2}\left[\frac{\omega+\omega_J}{(\omega-\omega_J)^2 + (\Delta\omega_J/2)^2}\right.$$
$$\left. + \frac{\omega-\omega_J}{(\omega+\omega_J)^2 + (\Delta\omega_J/2)^2}\right]. \qquad (14)$$
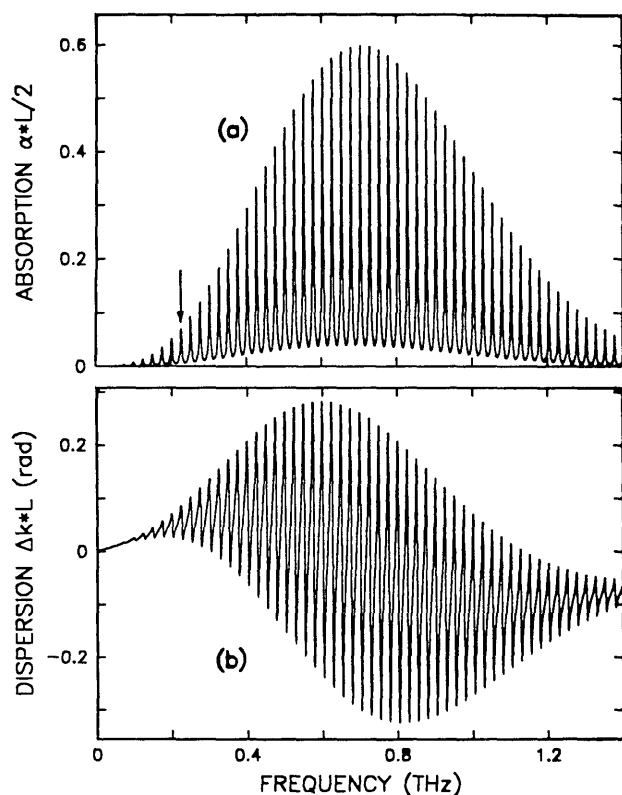
Fig. 6. (a) Calculated absorption and (b) dispersion in radians of 38.7 cm of 800 hPa of N_2O vapor.

The absorption and the dispersion over the whole spectral range of the terahertz pulse are found by a summation of Eqs. (10) and (13) over all transitions within this spectral width.

5. COMPARISON OF CALCULATIONS AND MEASUREMENTS

From molecular collision theories[19,20] and experimental studies of rovibronic lines in the ν_3 band[21] it is known that the linewidth $\Delta\omega_J$ varies slightly with rotational quantum number, showing smaller widths for increasing J. Over the central part of the spectrum excited by the terahertz pulses the linewidth decreases by 15% as J increases from 15 to 40.

For a quantitative calculation of the spectra, we assume the same linewidth variation as that found in Ref. 21 and then use a single transition as the reference line for the specification of the linewidth. The amplitude absorption $\alpha L/2$ and the phase change in radians, $\Delta k L$, calculated for a pressure $p = 800$ hPa and a cell length $L = 0.387$ m, are shown in Fig. 6, with the choice of constants $B_V = 12.56163$ GHz, $D_V = 5.279$ kHz, $\mu = 0.166 \times 3.33 \times 10^{-30}$ ampere-second-meter, and $f_0 = 0.89$ for room-temperature N_2O molecules. The only free parameter for the simulation of these spectra is the linewidth $\Delta\omega_J$ of the reference line, for which we use the transition $J = 8 \rightarrow 9$ occurring at 226.1 GHz and indicated by the arrow in Fig. 6. In this example the width of this transition was determined to be $\Delta\omega_{89} = 2\pi \times 4.93$ GHz. As Fig. 6 shows, with this linewidth the individual absorption lines start to overlap, causing significant absorption and phase shifts between the lines.

The experimental counterpart of Fig. 6 is shown in Fig. 7, obtained from the measured pulse of Fig. 3 by the method of time-domain spectroscopy.[12] For this method two measured pulse shapes are needed: the transmitted pulse (reference pulse) with no vapor in the cell [Fig. 4(a)] and the transmitted pulse with vapor in the cell [Fig. 3(a)]. Then, by means of the numerical Fourier transforms of these two pulses, indicated by the dashed and solid curves in Fig. 7(a), the amplitude absorption $\alpha L/2$ and the phase change $\Delta k L$ in radians due to the vapor are obtained, as shown in Figs. 7(b) and 7(c), respectively. All the complexities due to reflections cancel out in this procedure, which requires a stable reproducible reference pulse over relatively long time periods. Another technical problem involves the residual water vapor in the terahertz beam path. We have noticed that water vapor is gradually desorbed from the vapor cell, and the amount of water vapor is therefore not the same for the reference pulse and the transmitted pulse. This situation causes the appearance of water lines in the measured spectra of
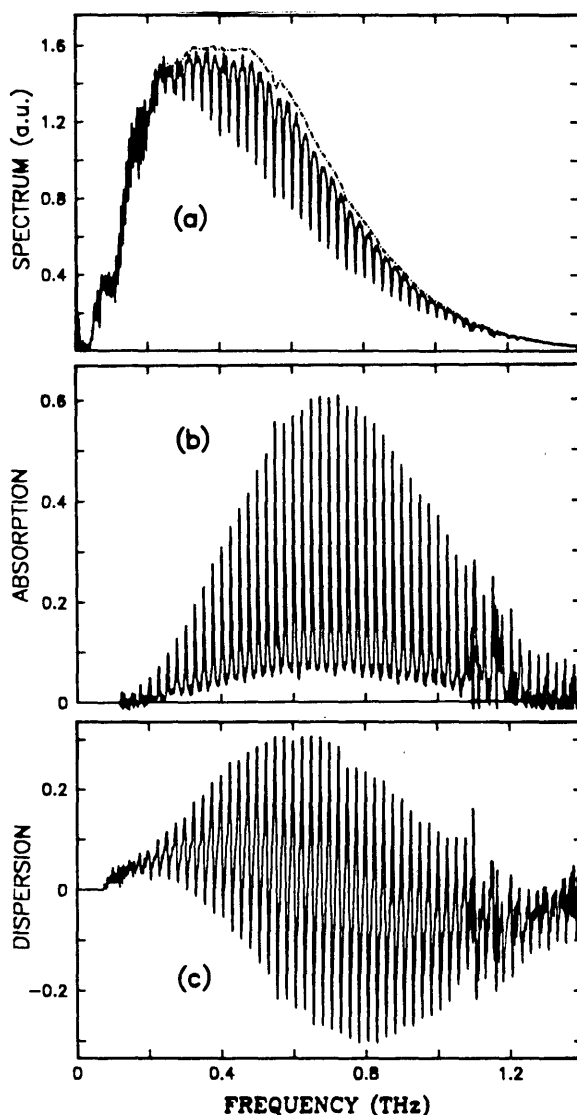

Fig. 7. (a) Fourier-transformed amplitude spectrum of the measured pulse from Fig. 3 (solid curve) and of the reference pulse (dashed curve), and the corresponding (b) absorption and (c) dispersion in radians.
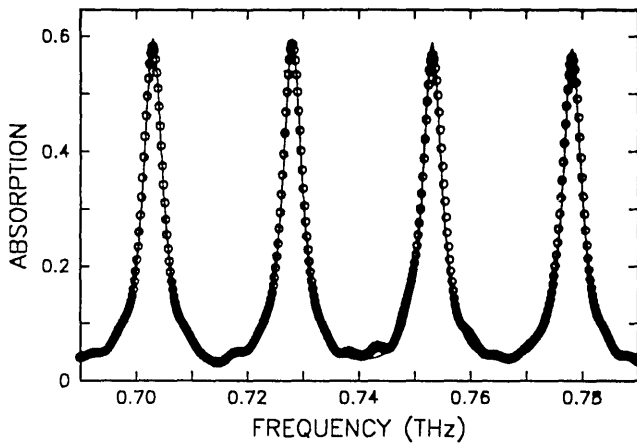
Fig. 8. Comparison of the Fourier-transformed measurement (circles) and calculation (solid curve) for the central part of the absorption spectrum of 800 hPa of N_2O vapor.

Fig. 7 and the appearance of additional time-domain oscillations in our measurements. As we can see in Fig. 7, the deviation at 0.6, 1.1, and 1.2 THz result from the strong water-vapor absorption lines at these frequencies; otherwise, the envelope and the absolute amplitudes of the spectral lines agree quite well with the calculation of Fig. 6. The central part of the spectrum of Fig. 7(b) is shown on a magnified frequency scale in Fig. 8, where the circles represent the measurement and the solid curve represents the calculation. This excellent agreement between theory and experiment for both amplitude and line shape was obtained with the linewidth as the only adjustable parameter. The resolution of these spectra, which is determined by the reciprocal of the maximum time delay, was increased by extending the scan range of Fig. 3(a) and the reference pulse artificially to 4.8 ns by the addition of zeros.

Within the limits of our frequency resolution the spectra presented in Figs. 7(b) and 7(c) could also be simulated quite well by the assumption of a constant linewidth for all the transitions. For this case the spectra are represented by an average width $\Delta\omega = 2\pi \times 4.4$ GHz, corresponding to the coherent relaxation time $T_2 = 72$ ps determined by the relationship $\Delta\omega = 2/T_2$. In comparison with Fig. 6, this assumption of an average linewidth causes some small deviations for lines at the low- and high-frequency limits of the spectra, while the central part remains unchanged.

If we know the spectral response, the propagation of the terahertz beam through the N_2O vapor can be obtained from Eq. (9) above. In actuality, our calculations are strictly numerical and are performed in the following manner. The reference pulse, as shown in Fig. 4(a), is assumed to be the input pulse to the vapor. This pulse is numerically Fourier analyzed. The individual frequency components are then multiplied by the amplitude absorption and the phase change as presented in Fig. 6 or as given in analytical detail in Section 4. Then the inverse numerical Fourier transform is performed, giving the predicted output pulse. The fact that the input pulse includes reflections, some effects that are due to residual water vapor, and system noise yields predicted output pulses that are remarkably similar to the actual observations, as we demonstrated above in Figs. 3(b), 4(d), and 5. The numerical simulations reproduce the measurements

in pulse shape and absolute amplitude, for the exciting pulse as well as for the coherently generated pulse train. This is again demonstrated by the comparison in Fig. 9 between experiment (solid curves) and theory (dashed curves) for the propagating and first reradiated coherent pulses, in which theory and experiment agree to within 1%. The agreement between theory and experiment is so precise that the two overlapping curves appear as a single curve.

Another example of a calculated spectrum is shown in Fig. 10 for a pressure of 120 hPa with the FWHM linewidth for the reference line of $\Delta\omega_{89} = 2\pi \times 747$ MHz. With this narrow linewidth the adjacent absorption lines do not significantly overlap, although a slight phase shift between the lines still remains. From these spectra the theoretical pulses as shown in Figs. 4(d) and 5 were derived. The additional oscillations seen in Fig. 5(c) result from a slightly different water concentration along the propagation length for the measurements with and without N_2O vapor in the cell, as we discussed above.

6. SELF-PRESSURE BROADENING

Only the linewidth $\Delta\omega_{89}$ as mentioned in Section 5 was adjusted to fit the theoretical pulse structures to the experimental data. Therefore an analysis of the measurements by the described theoretical model permits an accurate determination of the linewidth broadening that is due to the N_2O vapor pressure and hence of the coherent relaxation time T_2 even under conditions when adjacent
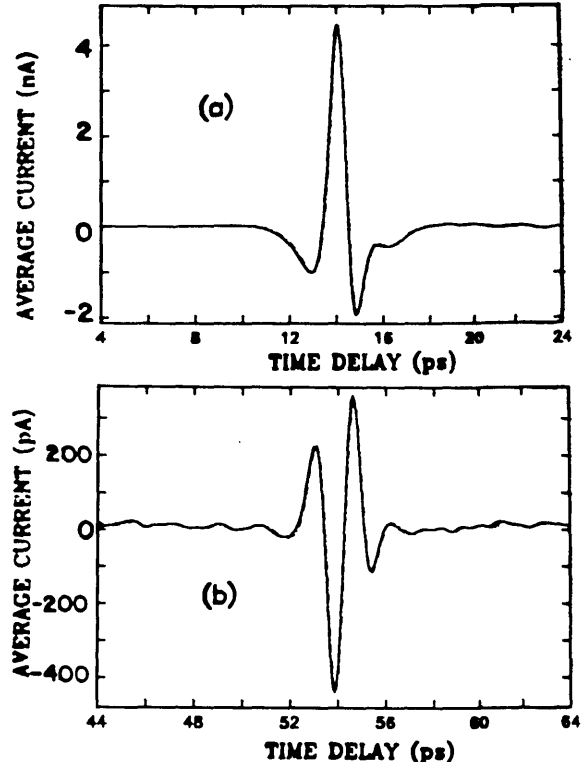

Fig. 9. Comparison of measured (solid curves) and calculated (dashed curves) (a) exciting pulse and (b) first reradiated coherent pulse after propagation through 38.7 cm of 800 hPa of N_2O vapor. The agreement between theory and experiment is so precise that the two overlapping curves appear as a single curve. These are the same results as those of Figs. 3(a) and 3(b) but are shown on expanded time scales.
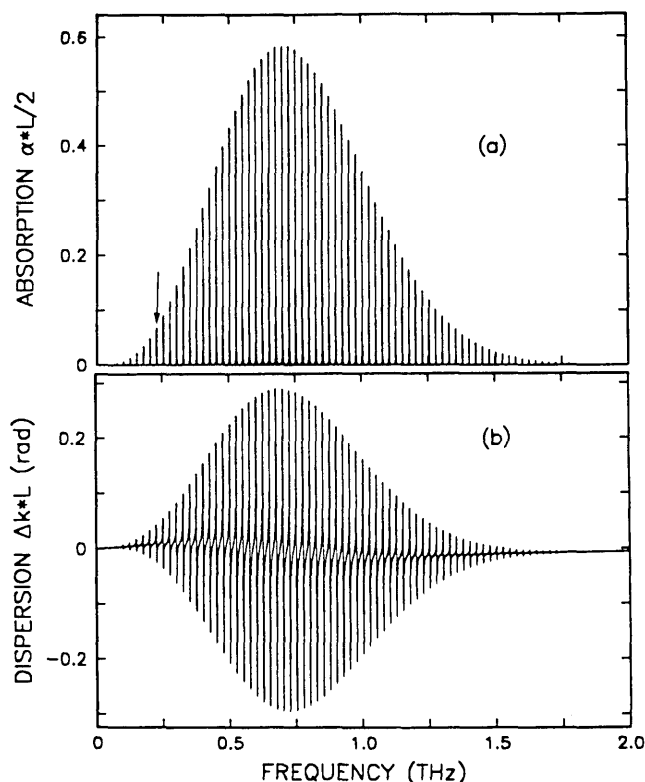
Fig. 10. Calculated spectra for (a) the amplitude absorption and (b) the dispersion in radians of a 38.7-cm length of 120 hPa of N_2O vapor.
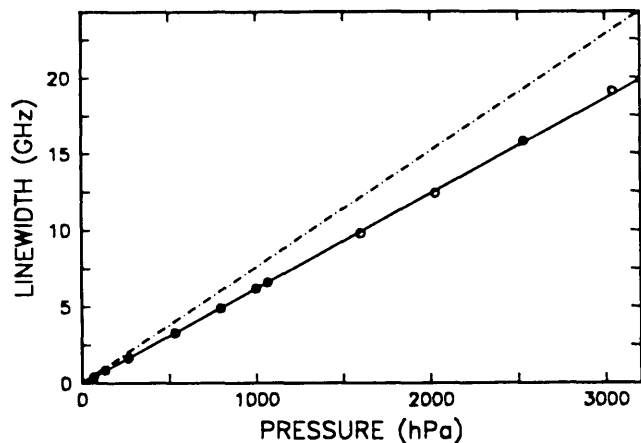

Fig. 11. Self-pressure broadening of N_2O as a function of the vapor pressure for the FWHM linewidth of the transition $J = 8 \rightarrow 9$ at 226.1 GHz. The solid line represents an interpolation through the measured points (circles); the dashed line would be obtained if propagation effects were neglected.

rotational levels in the frequency domain can barely be resolved. From the time-domain spectroscopy of water vapor,[10,11] which has a complicated series of incommensurate absorption lines, an average T_2 was obtained for pressure broadening by the buffer gases oxygen, nitrogen, and carbon dioxide.[11]

Similarly, from our measurements presented here, under normal conditions, only an average pressure broadening over all the excited rotational lines can be deduced. However, with the assumed linewidth variation as found in Ref. 21 the broadening of a definite line can be evaluated

and compared directly with frequency-resolving experiments measuring individual lines. The results of our measurements for the linewidth broadening of the transition $J = 8 \rightarrow 9$ occurring at 226.1 GHz are shown in Fig. 11 as a function of the N_2O pressure. The solid line represents an interpolation between the measured points (circles) and demonstrates a linear dependence of the FWHM linewidth over a pressure range of almost two orders of magnitude. At the higher pressure values the broadening already becomes as large as the line spacing and therefore causes a strong spectral overlap of adjacent transitions. This makes an accurate analysis of such data in the frequency domain quite difficult. From the slope of the solid line we evaluate a self-pressure broadening parameter for the $J = 8 \rightarrow 9$ transition at room temperature of $C_W = 6.20$ MHz/hPa $= 8.26$ MHz/Torr for the FWHM linewidth, which is in excellent agreement with the infrared measurements of Ref. 21 but is roughly 10% smaller than the value obtained from microwave experiments on the same transition.[22] For a temperature correction of the data a dependence of the form $C_W(T) = C_W(T_0)(T/T_0)^{-n}$, with $n = 0.96$ as found from Ref. 22, was used.

If propagation effects were neglected in the analysis of the pressure broadening, significantly larger linewidths would be obtained as indicated by the dashed line in Fig. 11. This discrepancy is due to absorption. Under our experimental conditions the peak spectral absorption $\alpha_{max}L/2$ cannot be assumed to be small compared with unity [see Figs. 6(a), 7(b), and 10(a)]. At the line center, saturation effects already become noticeable and cause an additional spectral broadening, which in the time domain is manifest as a faster exponential decay of the measured pulse train. This behavior can be seen in Fig. 12, where a calculated pulse train for 67-hPa N_2O pressure with $T_2 = 724$ ps (assuming a constant linewidth for all transitions) is shown together with an exponential decay having the same T_2 decay constant. It should be emphasized that the theory including propagation and centrifugal dephasing is in excellent agreement with experiment and allows for the determination of the linewidth to within a few percent. The irregular pattern in Fig. 12 is due to centrifugal dephasing, and the faster decay is mainly due to absorption saturation. As shown above in Fig. 4, these
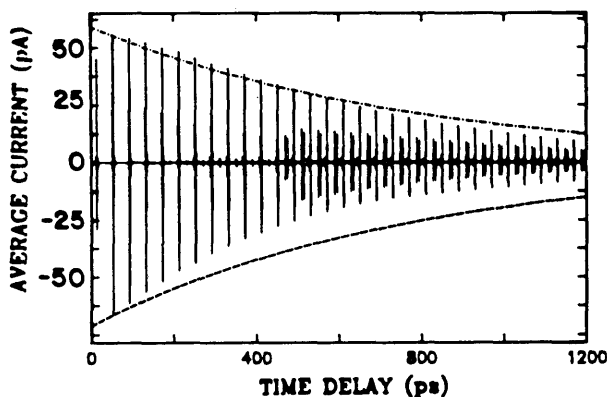

Fig. 12. Calculated FID signal from a 38.7-cm length of 67 hPa of N_2O vapor compared with a simple exponential decay having the same decay constant. The deviations result from propagation effects and centrifugal dephasing.
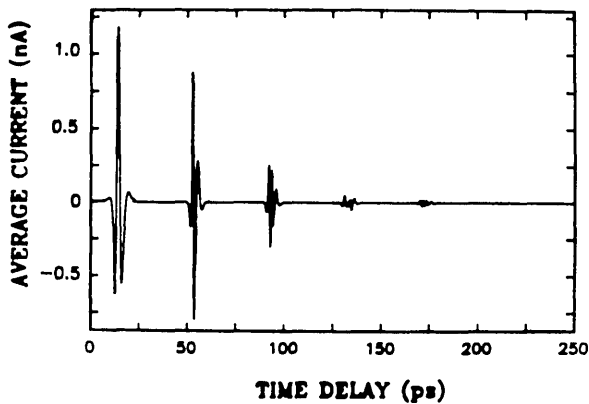
Fig. 13. Calculated transmitted pulse structure for the input pulses of Fig. 4(a) after propagation through 5.4 m of N_2O vapor at a pressure of 1013 hPa.

features agree in detail with experiment. The purpose of Fig. 12 is to show the deviation of the naïve assumption of a simple exponential decay with the complete theory. Because the linewidth is proportional to pressure, the absorption on line center is independent of pressure. This point is illustrated by the absorption curves shown in Figs. 6 and 10, where the peak absorptions remain the same even though the pressures have changed from 800 to 120 hPa. The only way to change the absorption is to change the length of the cell. With fixed T_2 (pressure), the apparent decay seen on the calculated FID pulse train becomes longer as the propagation length through the vapor becomes shorter. It approaches T_2 only for an optically thin sample, where the remaining deviations are due to the centrifugal dephasing.

While the absorptive influence on pulse propagation can clearly be observed, dispersive effects, which in addition to centrifugal dephasing could also cause a reshaping of the coherent pulses, are negligible under our conditions. Dispersive effects become important at larger delay times and particularly at longer absorption lengths, when the sample itself becomes an optically thick medium. This is illustrated by the numerical example presented in Fig. 13, which shows the calculated transmitted pulse structure for the input pulses of Fig. 4(a) after propagation through 5.4 m of N_2O vapor at a pressure of 1013 hPa. For this example $\alpha_{max}L/2 = 8.4$. Under these conditions the first reradiated coherent pulse is almost as large as the transmitted exciting pulse. In comparison with the results discussed above, the pulse train shows considerable reshaping from pulse to pulse, as determined by the strong dispersion of the vapor over this much longer propagation length. For such an optically thick medium the pulse propagation has entered the regime of the so-called zero-area (0π) pulse of coherent optics.[23]

With increasing vapor pressure a gradual shift of the entire measured pulse structure to longer delay times can be observed, owing to the increase of the nonresonant refractive index n with vapor density; e.g., a pressure of 3 atm (3039 hPa) causes a time shift of 1.97 ps. Using the reference pulse, taken without N_2O vapor in the cell, as input for the simulated pulse structure and fitting the theoretical pulse to measurements at higher pressures, we evaluate an index change of $\Delta n = 5.03 \times 10^{-7}$ hPa^{-1}.

7. CONCLUSION

We have experimentally and theoretically studied terahertz coherent transients. After excitation by a subpicosecond pulse of terahertz electromagnetic radiation, a N_2O vapor sample was observed to emit a train of subpicosecond terahertz pulses. The decaying train of subpicosecond pulses, separated from one another by 39.8 ps, extended to beyond 1 ns, and within the train the individual pulse shapes gradually changed. Because the experiments were performed in the low-intensity limit of the coupled Maxwell–Bloch equations, a linear dispersion theory analysis was used to compare theory with the observations. The resulting excellent agreement between theory and experiment permitted the determination of the frequency separation between the individual N_2O lines, the centrifugal stretching constant, and the coherent relaxation time T_2 as a function of vapor pressure, even for the case of strongly overlapping lines.

REFERENCES AND NOTES

1. See, e.g., A. Abragam, *The Principles of Nuclear Magnetism* (Oxford U. Press, New York, 1961).
2. N. A. Kurnit, I. D. Abella, and S. R. Hartmann, "Observation of a photon echo," Phys. Rev. Lett. **13**, 567 (1964).
3. See, e.g., L. Allen and J. H. Eberly, *Optical Resonance and Two-Level-Atoms* (Wiley, New York, 1975).
4. R. G. Brewer, "Coherent optical spectroscopy," in *Frontiers in Laser Spectroscopy*, R. Balian, S. Haroche, and S. Liberman, eds. (North-Holland, Amsterdam, 1977), p. 341.
5. R. L. Shoemaker, "Coherent transient infrared spectroscopy," in *Laser and Coherence Spectroscopy*, J. I. Steinfeld, ed. (Plenum, New York, 1978), p. 197.
6. H. Harde and H. Burggraf, "High precision level splitting measurements with picosecond light pulses from an injection laser," in *Coherence and Quantum Optics V*, L. Mandel and E. Wolf, eds. (Plenum, New York, 1984), p. 993.
7. H. Lehmitz, W. Kattau, and H. Harde, "Modulated pumping in Cs with picosecond pulse trains," in *Methods of Laser Spectroscopy*, Y. Prior, A. Ben-Reuven, and M. Rosenbluh, eds. (Plenum, New York, 1986), p. 97.
8. T. G. Schmalz and W. H. Flygare, "Coherent transient microwave spectroscopy and Fourier transform methods," in *Laser and Coherence Spectroscopy*, J. I. Steinfeld, ed. (Plenum, New York, 1978), p. 125.
9. M. van Exter, Ch. Fattinger, and D. Grischkowsky, "High brightness teraHz beams characterized with an ultrafast detector," Appl. Phys. Lett. **55**, 337 (1989).
10. M. van Exter, Ch. Fattinger, and D. Grischkowsky, "TeraHz time-domain spectroscopy of water vapor," Opt. Lett. **14**, 1128 (1989).
11. M. van Exter, Ch. Fattinger, and D. Grischkowsky, "Time-domain far-infrared spectroscopy of water vapor and direct measurement of collisional relaxation times," in *Laser Spectroscopy IX—Proceedings of the Ninth International Conference on Laser Spectroscopy*, M. S. Feld, J. E. Thomas, and A. Mooradian, eds. (Academic, San Diego, 1989).
12. D. Grischkowsky, S. Keiding, M. van Exter, and Ch. Fattinger, "Far-infrared time-domain spectroscopy with tera-

hertz beams of dielectrics and semiconductors," J. Opt. Soc. Am. B **7**, 2006 (1990).

13. M. van Exter and D. Grischkowsky, "Characterization of an optoelectronic teraHz beam system," IEEE Trans. Microwave Theory Tech. **38**, 1684 (1990).

14. M. Rosatzin, D. Suter, W. Lange, and J. Mlynek, "Phase and amplitude variations of optically induced spin transients," J. Opt. Soc. Am. B **7**, 1231 (1990).

15. K. L. Foster, S. Stenholm, and R. G. Brewer, "Interference pulses in optical free induction decay," Phys. Rev. A **10**, 2318 (1974).

16. M. Woerner, A. Seilmeier, and W. Kaiser, "Reshaping of infrared picosecond pulses after passage through atmospheric CO_2," Opt. Lett. **14**, 636 (1989).

17. A. G. Maki, J. S. Wells, and M. D. Vanek, "Heterodyne frequency measurements on N_2O near 930 cm^{-1}," J. Mol. Spectrosc. **138**, 84 (1989).

18. C. H. Townes and A. L. Schawlow, *Microwave Spectroscopy* (Dover, New York, 1975).

19. P. W. Anderson, "Pressure broadening in the microwave and infra-red regions," Phys. Rev. **76**, 647 (1949).

20. D. Robert and J. Bonamy, "Short range force effects in semiclassical line broadening calculations," J. Phys. **40**, 923 (1979).

21. M. Margottin-Maclou, P. Dahoo, A. Henry, and L. Henry, "Self-broadening parameters in the ν_3 band of N_2O," J. Mol. Spectrosc. **111**, 275 (1985).

22. J. M. Colmont and N. Semmoud-Monnanteuil, "Pressure broadening of the N_2O $J = 9 \leftarrow 8$ rotational transition by N_2O, N_2 and O_2," J. Mol. Spectrosc. **126**, 240 (1987).

23. J. E. Rothenberg, D. Grischkowsky, and A. C. Balant, "Observation of the formation of the 0π pulse," Phys. Rev. Lett. **53**, 552 (1984). This paper includes an extensive reference list pertaining to theory and experiments on the 0π pulse.

24. H. Harde, S. Keiding, and D. Grischkowsky, "The commensurate echoes: periodic rephrasing of molecular transitions in free-induction decay," Phys. Rev. Lett. **66**, 1834 (1991).